

Drastic Changes in Interfacial Hydrodynamics due to Wall Slippage: Slip-Intensified Film Thinning, Drop Spreading, and Capillary Instability

Ying-Chih Liao,¹ Yen-Ching Li,² and Hsien-Hung Wei^{2,*}

¹*Department of Chemical Engineering, National Taiwan University, Taipei 106, Taiwan*

²*Department of Chemical Engineering, National Cheng Kung University, Tainan 701, Taiwan*

(Received 3 January 2013; published 26 September 2013)

We report that wall slippage can drastically change both steady and dynamic flow characteristics for a wide class of free-surface thin film flows. This is demonstrated by (i) the breakdown of the 2/3 law and its replacement by a new quadratic law for the deposited film thickness in the Landau-Levich-Bretherton coating, (ii) the departure from de Gennes–Tanner’s cubic law for dynamic contact angles in drop spreading, consequently resulting in much faster spreading than the classical Tanner law, and (iii) the exaggerated capillary instability of an annular film where a fractional amount of wall slip can lead to much more rapid draining and hence make the film more vulnerable to rupture. In (ii), the molecular precursor film is shown to have a length varying like the $-1/2$ power of the spreading speed, producing an anomalous $1/3$ diffusion law governing its spreading dynamics. A variety of existing experimental findings can be well captured by the new scaling laws we derive. All these features are accompanied with no-slip-to-slip transitions, offering alternative means for probing slip boundaries.

DOI: [10.1103/PhysRevLett.111.136001](https://doi.org/10.1103/PhysRevLett.111.136001)

PACS numbers: 83.50.Lh

While the no-slip boundary condition is commonly used in most practical flows, the apparent breakdown of this condition can occur on a number of occasions such as flowing polymer liquids over smooth surfaces [1], pumping in hydrophobic microchannels [2], coating on chemically decorated planes [3], and wetting on heterogeneous or structured substrates [4]. Such wall slippage, intrinsic or apparent, is often described by the Navier slip condition, $u = \lambda du/dy$, with the slip length λ measuring the amount of slip through the ratio of the slip velocity to the local shear rate on a surface [5]. Apparently, surfaces with large λ reduce viscous drag and hence enable the speed up of flow.

Perhaps the most frequent use of the Navier condition appears in modeling interfacial flows involving moving contact lines [6]. In most situations, λ is much smaller than the liquid thickness h . So slip effects are merely important near the contact line to aid in relieving the stress singularity, but do not change the macroscopic flow characteristics (see Refs. [7–9] for more comprehensive reviews). However, there might be situations, for instance, like those involving polymer liquids [10], where slip lengths could be so large that the influence of wall slip can penetrate the entire bulk flow. In this case, the flows will be speeded up by a factor of λ/h . This flow amplification would not only change flow characteristics, but also dramatically modify how the fluid-fluid interfaces act both temporally and spatially in response to the flows. In this Letter we will demonstrate such effects on three closely related interfacial flow problems: (i) Landau-Levich-Bretherton coating, (ii) forced wetting and liquid spreading, and (iii) capillary instability of annular films. As will be shown, not only will many scaling laws based on the no-slip condition be replaced by new ones due to strong wall

slippage, but also a variety of experimental findings can be captured by these new laws.

Breakdown of the Landau-Levich-Bretherton law.—When a long bubble displaces liquid in a small capillary tube, a thin liquid film can be deposited on the interior wall of the tube. This is the classical Bretherton problem [11]. The similar film deposition can also be realized by pulling a plate out of a bath of liquid, as studied long ago by Landau and Levich [12]. This so-called Landau-Levich-Bretherton (LLB) coating possesses most of the features seen in many practical coating flows [13]. The main feature of the LLB problem is that the deposited film thickness h varies with the coating speed U according to the well-known 2/3 law [11,12],

$$h/R \sim Ca^{2/3}, \quad (1)$$

where $Ca = \mu U/\gamma$ ($\ll 1$) is the capillary number with γ being the surface tension, and R is the radius of the capillary tube (or the round meniscus). This 2/3 law is obtained by balancing the capillary pressure and viscous shear stress under the no-slip condition. When wall slip exists, it tends to increase the capillary draining *out* of the film and thereby makes the film thinner. So when decreasing Ca in Eq. (1) to the point where $h \sim \lambda$, the 2/3 law breaks down at the critical capillary number,

$$Ca_c \sim (\lambda/R)^{3/2}. \quad (2)$$

Further decreasing Ca below Ca_c , a new coating law must emerge to govern the behavior of h below λ in this strong slip regime. Therefore, Ca_c marks the transition point from no slip to strong slip. The same transition point has also been observed experimentally for dip coating over textured surfaces [14].

To derive the new coating law in the strong slip regime ($h < \lambda$), we start with the velocity scale of the capillary draining: $u_{\text{cap}} \sim (h/\ell)^3(\gamma/\mu)$, obtained by balancing the capillary pressure force $p/\ell \sim \gamma h/\ell^3$ to the viscous force (per unit depth) $\mu u_{\text{cap}}/h^2$ over the transition zone of size $\ell \sim (hR)^{1/2}$ between the uniform film and the round meniscus [see Fig. 1(a)]. Wall slip amplifies the above velocity to $(\lambda/h)u_{\text{cap}}$ and, hence, further thins the film. Balancing this velocity to the coating speed U gives a new quadratic law for $h < \lambda$ when $\text{Ca} < \text{Ca}_c$:

$$h/R \sim \text{Ca}^2(R/\lambda)^2. \quad (3)$$

Note that in deriving Eq. (3), we require $u_{yy} \gg u_{xx}$ to ensure the standard lubrication approximation $p_x = \mu u_{yy}$ along the flow direction (where the subscripts denote spatial derivatives in either the flow direction x , or the transverse direction y). Since $u_{xx} \sim (\lambda/h)u_{\text{cap}}/\ell^2$ can be best estimated from the plug flow, the above criterion yields $u_{\text{cap}}/h^2 \gg (\lambda/h)u_{\text{cap}}/\ell^2$ (using $p_x \gg \mu u_{xx}$ and $p \sim \gamma h/\ell^2$). So the analysis here is only valid for

$$\lambda h/\ell^2 \ll 1 \quad \text{or} \quad \lambda/R \ll 1. \quad (4)$$

To test the new scalings (2) and (3), we derive the following lubrication equation and numerically determine

the deposited film thickness h_∞ : $(h^3 + 3\lambda h^2)h_{xxx} = 3\text{Ca}(h - h_\infty)$ with $h = h_\infty$ and $h_x = h_{xx} = 0$ as $x \rightarrow -\infty$, and $h_{xx} = 1/R$ as $x \rightarrow \infty$ [15]. The calculated h_∞ [Fig. 1(b)] and Ca_c [Fig. 1(c)] indeed confirm the scaling laws shown above.

In fact, such slip-intensified film thinning can be best explained by apparent viscosity: $\mu_{\text{app}} = \mu h/(h + \lambda)$, which can be defined through the ratio of the viscous stress on a slippery surface $\mu U/(h + \lambda)$ to the shear rate U/h as if the surface were no slip. Replacing μ by μ_{app} in the LLB law (1) leads to

$$h/R \sim (\mu_{\text{app}}U/\gamma)^{2/3}. \quad (5)$$

This is actually the *effective* LLB law capable of unifying both the 2/3 law (1) in the no-slip limit ($h \gg \lambda$) and the quadratic law (3) in the strong slip limit ($h < \lambda$). As indeed, all the data in Fig. 1(b) can be successfully collapsed according to Eq. (5) [see Fig. 1(d)].

If slip effects are so strong that $u_{xx} \gg u_{yy}$ in violation of Eq. (4) due to either large λ or small R , the film would behave like a plug flow in which the pressure force can only be dissipated by the lateral viscous force via $p_x = \mu u_{xx}$, giving $\gamma h/\ell^3 \sim \mu U/\ell^2$ and thereby

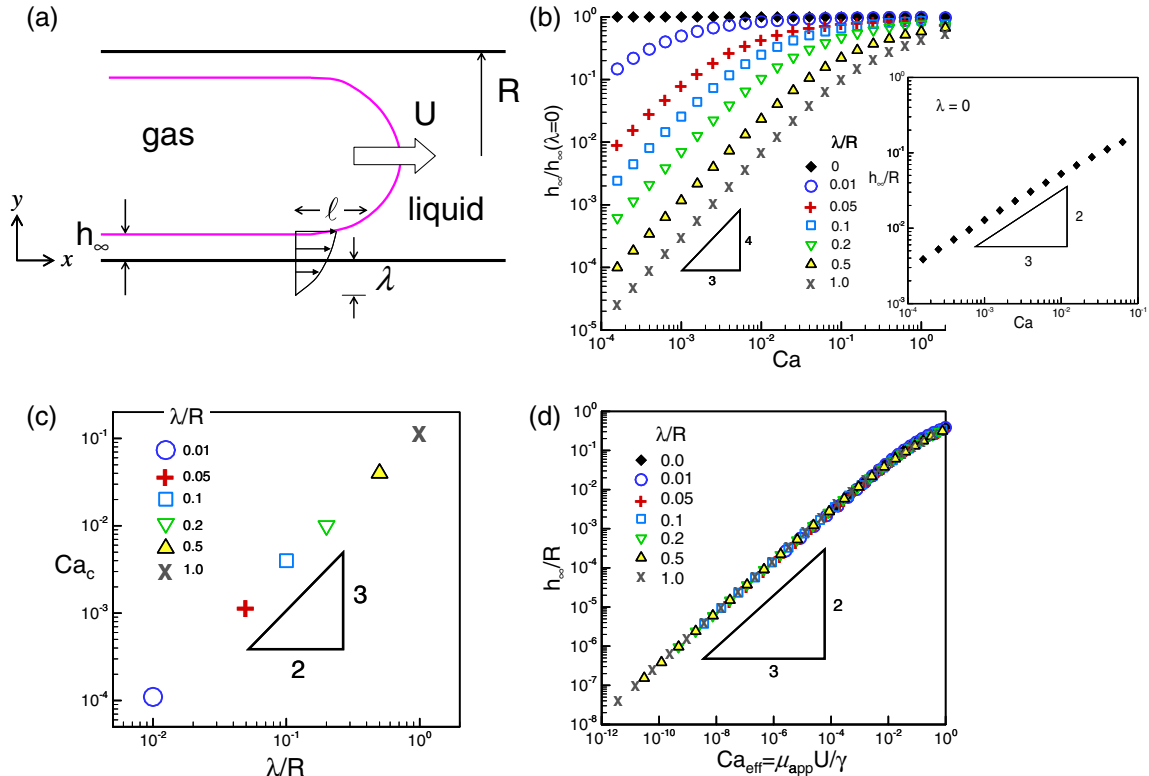


FIG. 1 (color online). (a) Flow geometry for bubble displacement in a slippery capillary. (b) Plot of the film thickness ratio $h_\infty/h_\infty(\lambda = 0)$ against Ca for various values of λ/R . Departure from the LLB 2/3 law (inset) is apparent when Ca is below some critical value Ca_c (estimated at $h_\infty/h_\infty(\lambda = 0) = 0.1$). In the small Ca regime $h_\infty/h_\infty(\lambda = 0) \propto \text{Ca}^{4/3}$, giving $h_\infty \propto \text{Ca}^2$ in agreement with Eq. (3). (c) The dependence of Ca_c on λ/R confirms Eq. (2). (d) All the data can be successfully collapsed according to the effective 2/3 law (5). For comparison, the results for $\lambda/R = 0.5$ and 1.0 are also calculated, though the lubrication approximation might not hold. Nevertheless, the actual results should not look qualitatively different from what we see here.

$$h/R \sim Ca^2. \quad (6)$$

So in this super slippage regime, Eq. (6) again shows a quadratic dependence on Ca but now is independent of λ .

Modified wetting and spreading laws due to wall slip.—It has been shown by Stone and others [13,16] that the LLB scalings can be used to derive relevant scaling laws for drop spreading problems in connection to the *apparent* dynamic contact angle $\theta_d \sim h/\ell$, since these two problems are hydrodynamically similar [17]. Now consider a spreading droplet of height h and radius r under the perfect wetting condition. In the no-slip limit ($h \gg \lambda$), the well-known de Gennes–Tanner law [7] and Tanner’s law [18] can be obtained by setting $\theta_d \sim h/\ell \sim (h/R)^{1/2}$ using the LLB law (1) with $\ell \sim r$ and $R \sim r/\theta_d$ being the radius of the curvature of the droplet,

$$\theta_d^3 \sim Ca, \quad (7a)$$

$$r \sim (t\Omega^3\gamma/\mu)^{1/10}. \quad (7b)$$

Equation (7b) is due to the constant volume constraint $\Omega = hr^2 \sim \theta_d r^3$ and $U \sim r/t$, where t is time.

If a droplet is placed on a slippery surface and its spreading starts with $h > \lambda$, Eqs. (7a) and (7b) hold only up to $h \sim \lambda$. When the droplet spreads to the point where h is smaller than λ , we enter the strong slip regime and new wetting and spreading laws can be derived from Eq. (3),

$$\theta_d^2 \sim Ca(r/\lambda), \quad (8a)$$

$$r \sim (t\Omega^2\lambda\gamma/\mu)^{1/8}. \quad (8b)$$

Equation (8a) can also be obtained by balancing the spreading force $\gamma\theta_d^2$ to the viscous drag $(\mu U/\lambda)r$ over λ for a liquid wedge near the contact line, similar to what de Gennes did for the no-slip case [7]. The crossover between Eqs. (7a) and (8a) gives the no-slip-to-slip transition point $Ca^* \sim (\lambda/r)^3$ below which Eq. (8a) governs the spreading behavior in the strong slip regime. This transition also agrees with the experimental data (see Fig. 2) reported by Chen [19] for spreading of a very viscous polymer liquid. According to de Gennes and co-workers [7,10], λ here can be as large as $10 \mu\text{m}$ owing to high degree of polymerization $N \sim 10^3$ used in Chen’s experiment [19]. For $r \sim 1 \text{ mm}$ used in Chen’s experiment, we can use $Ca^* \approx 3 \times 10^{-5}$ to estimate the slip length as $\lambda \sim 10 \mu\text{m}$, in agreement with the value estimated by de Gennes. In terms of spreading dynamics, compared to (7b) the droplet can now spread according to the slightly faster 1/8 law (8b), in good agreement with $r \propto t^{0.13}$ in experiments using picoliter polydimethylsiloxane (PDMS) drops [20].

It is worth mentioning that a quite similar wetting law like Eq. (8a) can also be found by incorporating the diffuse interface theory into the moving contact line problem [21]. In this approach, fluid slip comes from the uncompensated Young stress due to the deviation of the microscopic contact angle θ_m to its equilibrium value θ_e . The resulting contact angle relationship is found to be $\cos\theta_e = \cos\theta_m + \xi Ca/\lambda$ (with ξ being the thickness of the interface), which

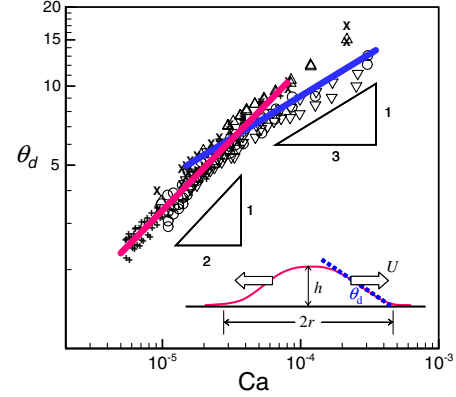


FIG. 2 (color online). Measured apparent dynamic contact angle θ_d (in degrees) vs. Ca for spreading of very viscous silicone oil in Ref. [19]. Symbols are data at different runs. Departure from the de Gennes–Tanner law $\theta_d \sim Ca^{1/3}$ (best fit: $\theta_d = 201.3 Ca^{0.33}$, thick blue line) becomes apparent for $Ca < 3 \times 10^{-5}$ in which $\theta_d \propto Ca^{1/2}$ (best fit: $\theta_d = 1674.3 Ca^{0.54}$, thin pink line) as predicted by Eq. (8a).

has been confirmed by extensive computer simulations [22]. If θ_m and θ_e are small, the above relationship is reduced to $\theta_m^2 \approx \theta_e^2 + 2\xi Ca/\lambda$ [8] similar to Eq. (8a). There is no surprise about this similarity because in both cases the capillary forces are dissipated by the same viscous stress $\mu U/\lambda$ across the slip length λ .

If a much smaller droplet is used or λ is large such that $\lambda \geq R$ in violation of Eq. (4), the spreading in this super slippage regime will be driven by a plug flow according to Eq. (6), giving

$$\theta_d \sim Ca, \quad (9a)$$

$$r \sim (t\Omega\gamma/\mu)^{1/4}. \quad (9b)$$

Equation (9a) is again the result by balancing the spreading force $\gamma\theta_d^2$ to the viscous force $\mu(U/r)h$ on the lateral side of the droplet around its periphery [23]. This leads to the much faster 1/4 law (9b), as derived in Ref. [23] as well as observed experimentally in Ref. [24] for drop spreading over a less viscous film (of viscosity μ_s) where the apparent slip length $\lambda \sim h\mu/\mu_s$ is large [25]. The same 1/4 law has also been observed in liquid spreading on micropillar arrays [26]. The corresponding dynamic contact angle behaves as $\theta_d \propto r^{-3} \propto t^{-3/4}$, as identified in similar experiments by MacHale and his co-workers [27]. A change from Tanner’s $-3/10$ law to the $-3/4$ law for θ_d —an indication of the no-slip-to-slip transition—was also observed in the same report [27].

As shown above, at the macroscopic level, droplets can spread according to the new scaling laws (8) and (9) due to strong wall slip. We should emphasize that these laws are derived from the new LLB scalings (3) and (6) consistent with de Gennes’s local dissipation approach [7]. Unlike non-Tanner-like spreading due to other mechanisms [8], various results seen in drop spreading experiments can now be well captured by these laws and explained solely by wall

slip effects. At the meso- or microscopic level, we also want to explore how wall slip modifies the structure of the precursor film. It has been suggested that the disjoining pressure in the spreading precursor film on a no-slip surface can produce effects like wall slip to relieve the contact-line singularity [16]. So when wall slip is present, because of its coupling to disjoining pressure, the precursor film might have a rather different structure than that without slip. To see this, we restrict our attention to the strong slip regime with $h < \lambda (\ll R)$, and examine the corresponding *inner* flow behavior near the contact line. It can be shown that the pertaining equation (in the frame moving with the contact line) now reads

$$\text{Ca} h = -\lambda h^2 h_{xxx} + 3a^2 \lambda h_x / h^2, \quad (10)$$

where $a = (A/6\pi\gamma)^{1/2}$ is the molecular length to characterize disjoining pressure $\Pi = A/6\pi h^3$ with A being the Hamaker constant [7]. At the macroscopic scale where disjoining pressure is unimportant, Eq. (10) recovers scaling (8a). The thickness h_f and length L_f of the precursor film can be estimated by balancing the terms in Eq. (10). Balancing the surface tension h_{xxx} term to the viscous Ca term (i.e., matching θ_d given by Eq. (8a) to the microscopic contact angle due to the film) gives $(h_f/L_f)^2 \sim \text{Ca}(L_f/\lambda)$. Together with $(a/h_f)^2 \sim \text{Ca}(L_f/\lambda)$ obtained by balancing the disjoining pressure term to the viscous term, we find

$$h_f \sim a(\lambda/a)^{1/4} \text{Ca}^{-1/4} \quad (11a)$$

and

$$L_f \sim a(\lambda/a)^{1/2} \text{Ca}^{-1/2}, \quad (11b)$$

which are quite distinct from $h_f \sim a/\text{Ca}^{1/3}$ and $L_f \sim a/\text{Ca}^{2/3}$ found for perfectly wetting liquids on no-slip surfaces [7,28]. It should be noted that while wall slip can promote the film thinning due to capillary draining, it also helps the film thickening due to disjoining pressure. Because of this reason, both h_f and L_f predicted by (11a) and (11b) can be greater than those in the no-slip case if λ

is sufficiently large such that $(\lambda/a)^3 \text{Ca} > 1$. This might happen to spreading of polymer liquids. For instance, for $\lambda \sim 1 \mu\text{m}$, $a \sim 1 \text{ \AA}$, and $\text{Ca} \sim 10^{-5}$, the estimated film dimensions are $h_f \sim 20 \text{ nm}$ and $L_f \sim 3 \mu\text{m}$, which might be detectable in experiments. Perhaps the most distinctive feature here is that the film, because of (11b), will propagate like $L_f \propto t^{1/3}$ in an anomalous diffusion manner, in contrast to $L_f \propto t^{1/2}$ for diffuse films commonly seen in experiments [29]. A recent experimental study on spreading of polymer droplets found $L_f \propto t^\nu$ with ν varying from 0.31 to 0.42 [30], which can be well captured by $L_f \propto t^{1/3}$ for strong slip and $L_f \propto t^{2/5}$ from the no-slip scaling $L_f \sim a/\text{Ca}^{2/3}$ [7,28], respectively. The transition between these two distinct spreading behaviors can then be interpreted as a consequence of the no-slip-to-slip transition.

Exaggerated capillary instability of annular film.—If coating occurs inside a small capillary or around a fiber (of radius R), the film (of thickness h) might undergo capillary instability and can be susceptible to rupture [31]. Similar to Ref. [31], we derive the following equation governing the interface's dynamics:

$$h_t + (\gamma/3\mu)[(h^3 + 3\lambda h^2)(h_x/R^2 + h_{xxx})]_x = 0. \quad (12)$$

It is clear that the slip term can increase the linear growth rate by a factor of $3\lambda/h_0$, where h_0 is the unperturbed film thickness. It is also easily shown that the most unstable wavelength $L = 2^{3/2}\pi R$ does not change with λ in the linear instability regime. But as interface deflections grow with time due to capillary instability, the interface gradually develops into growing lobes alongside with shrinking necks [see Fig. 3(a)], so the gap in between—the thinnest part of the film h_{\min} —can see more influence from the slippery wall. Therefore, in the nonlinear regime, because of the factor λ/h_{\min} amplification in the capillary flow, we expect that the draining behavior here should differ qualitatively from the no-slip case.

Figure 3(b) shows how the calculated h_{\min} decreases with time t . For $\lambda = 0$, we find $h_{\min} \sim t^{-2/3}$ for intermediate

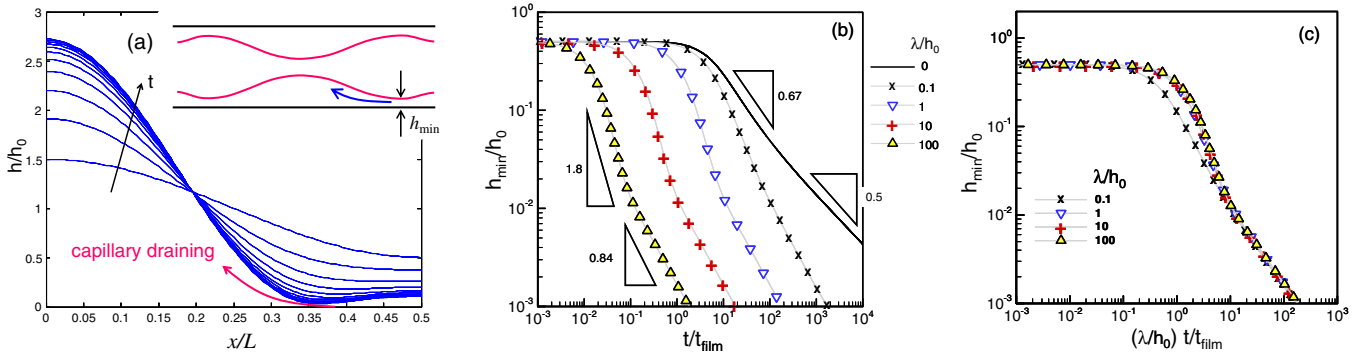


FIG. 3 (color online). (a) Typical spatiotemporal evolutions for the film thickness h (normalized by the unperturbed value h_0). $\lambda/h_0 = 0.5$. Time interval = 1 in units of $t_{\text{film}} = \mu R^4 / \gamma h_0^3$. The initial perturbation has amplitude $0.5 h_0$ and wavelength $L = 2^{3/2}\pi R$. (b) Plot of h_{\min}/h_0 against t/t_{film} . For $\lambda/h_0 > 0.1$, the thinning dynamics follow $h_{\min} \propto t^{-1.8}$ and $h_{\min} \propto t^{-0.84}$, much more rapid than $h_{\min} \propto t^{-0.67}$ and $h_{\min} \propto t^{-0.5}$ in the no-slip case. (c) Replot of (b) against the rescaled time $(\lambda/h_0)t/t_{\text{film}}$, showing collapse of the data for $\lambda/h_0 \geq 1$.

times followed by $h_{\min} \sim t^{-1/2}$ for long times, in accordance with Ref. [31]. Wall slip makes the draining much more accelerated. With λ more than 10% of the unperturbed film thickness h_0 , the intermediate and long time behaviors turn into $h_{\min} \sim t^{-1.8}$ and $h_{\min} \sim t^{-0.84}$, respectively. This means that with a fraction of wall slip, the film might become much more vulnerable to rupture than the no-slip case. Although we are still not clear about how slip effects lead to these power law changes, Fig. 3(c) shows that all the data for $\lambda/h_0 \geq 1$ can be collapsed by stretching the time scale by a factor of λ/h_0 , suggesting that the slip term λh^2 in Eq. (12) does control the long-term draining behavior.

To sum up, we have demonstrated that wall slip can significantly modify both steady and dynamic flow characteristics for a broad class of thin film flows. A number of existing experimental findings [14,19,20,24,26,27,30] can be well captured by new scaling laws we derive, suggesting that various phenomena can be universally interpreted in terms of wall slip effects. Unique no-slip-to-slip transitions can also be used to quantify the extent of wall slip, providing alternative means for probing slip boundaries.

This work is supported by the National Science Council of Taiwan.

*Corresponding author.

hhwei@mail.ncku.edu.tw

- [1] P.G. de Gennes, C.R. Acad. Sci., Ser. B **288**, 219 (1979).
- [2] D. C. Tretheway and C. D. Meinhard, *Phys. Fluids* **14**, L9 (2002).
- [3] V. S. J. Craig, C. Neto, and D. R. M. Williams, *Phys. Rev. Lett.* **87**, 054504 (2001).
- [4] C.-H. Choi and C.-J. Kim, *Phys. Rev. Lett.* **96**, 066001 (2006).
- [5] E. Lauga, M. P. Brenner, and H. A. Stone, *Handbook of Experimental Fluid Mechanics* (Springer, New York, 2007).
- [6] L. M. Hocking, *J. Fluid Mech.* **79**, 209 (1977); R. G. Cox, *ibid.* **168**, 169 (1986).
- [7] P. G. de Gennes, *Rev. Mod. Phys.* **57**, 827 (1985).
- [8] D. Bonn, J. Eggers, J. Indekeu, J. Meunier, and E. Rolley, *Rev. Mod. Phys.* **81**, 739 (2009).
- [9] J. H. Snoeijer and B. Andreotti, *Annu. Rev. Fluid Mech.* **45**, 269 (2013).
- [10] F. Brochard-Wyart, P. G. de Gennes, H. Hervet, and C. Redon, *Langmuir* **10**, 1566 (1994).
- [11] F. P. Bretherton, *J. Fluid Mech.* **10**, 166 (1961). For a common fluid in a capillary of size $R \sim 100 \mu\text{m}$, the estimated Bond number is $\text{Bo} = \rho g R^2 / \gamma \sim 10^{-2}$ based on the fluid density $\rho \sim 1 \text{ g/cm}^3$, surface tension $\gamma \sim 10 \text{ dyne/cm}$, and gravitational acceleration $g \sim 10^3 \text{ cm/s}^2$. So gravity effects are negligible.
- [12] L. Landau and B. Levich, *Acta Physicochim. URSS* **17**, 42 (1942).
- [13] H. A. Stone, *J. Fluid Mech.* **645**, 1 (2010); despite different geometries, the flows in these two problems can be described in a virtually identical manner. See also P. G. de Gennes, F. Brochard-Wyart, and D. Quéré, *Capillarity and Wetting Phenomena* (Springer, New York, 2003).
- [14] J. Seiwert, C. Clanet, and D. Quéré, *J. Fluid Mech.* **669**, 55 (2011). Because the surface structure here consists of arrays of micropillars and the deposited film tends to be thickened by more viscous forces imparted by these pillars, the pillar height h_p in effect acts like a “negative” effective slip length that tends to *slow down* the flow instead of speeding up. Nevertheless, the breakdown point of the LLB law occurs at $h \sim h_p$ and takes the same scaling form as Eq. (2).
- [15] In deriving this equation, similar to Ref. [11] we first determine the film velocity profile $u = G[y^2 - 2(y + \lambda)h]/2\mu$ that satisfies $u = \lambda \partial u / \partial y$ at the slippery wall $y = 0$ and $\partial u / \partial y = 0$ at the interface $y = h$, where $G = \partial p / \partial x$ is the pressure gradient generated by the Laplace pressure $p \approx -\gamma h_{xx}$. Because of fluid mass conservation, the equation can then be derived by equating the capillary flow rate $Q = -G(h^3 + 3\lambda h^2)/3\mu$ to the bubble sweeping rate $U(h - h_\infty)$.
- [16] S. Kalliadasis and H.-C. Chang, *Phys. Fluids* **6**, 12 (1994); *Ind. Eng. Chem. Res.* **35**, 2860 (1996).
- [17] The rationale behind this is that the flow in the *outer* wedge region away from the moving contact line resembles that in the transition region in the LLB problem—both merely involve the balance between surface tension and viscous forces. But this hydrodynamic analogy is only valid for perfectly wetting liquids or spreading over pre-existing films. Microscopic natures of the contact line only contribute logarithmic corrections to wetting dynamics (see, e.g., Refs. [8,9,16,28]).
- [18] L. H. Tanner, *J. Phys. D* **12**, 1473 (1979).
- [19] J.-D. Chen, *J. Colloid Interface Sci.* **122**, 60 (1988). According to Refs. [7,10], the slip length here can be estimated as $\lambda \sim a_m N^3 / N_e^2$, with $a_m \sim 0.1 \text{ nm}$ the molecular size, $N \sim 10^3$ and the degree of entanglement $N_e \sim 10^2$.
- [20] U. Albrecht, A. Otto, and P. Leiderer, *Phys. Rev. Lett.* **68**, 3192 (1992).
- [21] T. Qian, X.-P. Wang, and P. Sheng, *Phys. Rev. E* **68**, 016306 (2003); *J. Fluid Mech.* **564**, 333 (2006).
- [22] W. Ren and W. E, *Phys. Fluids* **19**, 022101 (2007).
- [23] F. Brochard-Wyart, G. Debrégeas, and P. G. de Gennes, *Colloid Polym. Sci.* **274**, 70 (1996).
- [24] L. Bacri, G. Debrégeas, and F. Brochard-Wyart, *Langmuir* **12**, 6708 (1996).
- [25] O. I. Vinogradova, *Langmuir* **11**, 2213 (1995).
- [26] S. J. Kim, M.-W. Moon, K.-R. Lee, D.-Y. Lee, Y. S. Chang, and H.-Y. Kim, *J. Fluid Mech.* **680**, 477 (2011).
- [27] G. McHale, N. J. Shirtcliffe, S. Aqil, C. C. Perry, and M. I. Newton, *Phys. Rev. Lett.* **93**, 036102 (2004).
- [28] J. Eggers and H. A. Stone, *J. Fluid Mech.* **505**, 309 (2004). These scalings can be found using the same way to derive (11a) and (11b). Also, $h_f \sim (aL_f)^{1/2}$ always holds with and without slip.
- [29] H. Xu, D. Shirvanyants, K. Beers, K. Matyjaszewski, M. Rubinstein, and S. S. Sheiko, *Phys. Rev. Lett.* **93**, 206103 (2004).
- [30] C. M. Mate, *Langmuir* **28**, 16821 (2012).
- [31] P. S. Hammond, *J. Fluid Mech.* **137**, 363 (1983). Similar to Ref. [15], Eq. (12) can be derived using $h_t + Q_x = 0$ with $p \approx -\gamma(h/R^2 + h_{xx})$.